Environmental Science & Technology

pubs.acs.org/est

Article

Reactive Oxygen Species and Chromophoric Dissolved Organic Matter Drive the Aquatic Photochemical Pathways and Photoproducts of 6PPD-quinone under Simulated High-Latitude Conditions

Zachary C. Redman,* Jessica L. Begley, Isabel Hillestad, Brian P. DiMento, Ryan S. Stanton, Alon R. Aguaa, Michael C. Pirrung, and Patrick L. Tomco

Cite This: *Environ. Sci. Technol.* 2023, 57, 20813−20821

Read Online

ACCESS | Metrics & More | Article Recommendations | Supporting Information

Downloaded via UNIV CLERMONT AUVERGNE on December 15, 2023 at 15:08:55 (UTC).
See https://pubs.acs.org/sharingguidelines for options on how to legitimately share published articles.

ABSTRACT: The photochemical degradation pathways of 6PPD-quinone (6PPDQ, 6PPD-Q), a toxic transformation product of the tire antiozonant 6PPD, were determined under simulated sunlight conditions typical of high-latitude surface waters. Direct photochemical degradation resulted in 6PPDQ half-lives ranging from 17.5 h at 20 °C to no observable degradation over 48 h at 4 °C. Sensitization of excited triplet-state pathways using Cs^+ and Ar purging demonstrated that 6PPDQ does not decompose significantly from a triplet state relative to a singlet state. However, assessment of processes involving reactive oxygen species (ROS) quenchers and sensitizers indicated that singlet oxygen and hydroxyl radical do significantly contribute to the degradation of 6PPDQ. Investigation of these processes in natural lake waters indicated no difference in attenuation rates for direct photochemical processes at 20 °C. This suggests that direct photochemical degradation will dominate in warm waters, while indirect photochemical pathways will dominate in cold waters, involving ROS mediated by chromophoric dissolved organic matter (CDOM). Overall, the aquatic photodegradation rate of 6PPDQ will be strongly influenced by the compounding effects of environmental factors such as light screening and temperature on both direct and indirect photochemical processes. Transformation products were identified via UHPLC-Orbitrap mass spectrometry, revealing four major processes: (1) oxidation and cleavage of the quinone ring in the presence of ROS, (2) dealkylation, (3) rearrangement, and (4) deamination. These data indicate that 6PPDQ can photodegrade in cool, sunlit waters under the appropriate conditions: $t_{1/2}$ = 17.4 h tono observable decrease (direct); $t_{1/2}$ = 5.2−11.2 h (indirect, CDOM).

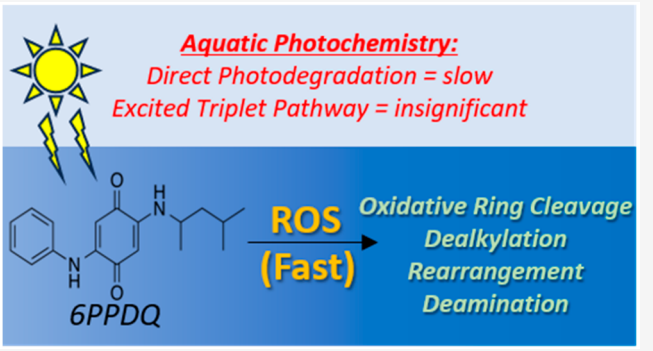

KEYWORDS: *Singlet Oxygen, Hydroxyl Radical, Photolysis, Photochemistry, Transformation Products, 6PPDQ, 6PPD-Q*

1. INTRODUCTION

Subarctic aquatic ecosystems are among the most sensitive on the planet to anthropogenic factors such as environmental contamination, which is having cumulative effects that negatively influence its structure, function, and sustainability.[1] The Subarctic is home to highly productive aquatic ecosystems that support many terrestrial and aquatic species that have cultural, subsistence, and economic significance. Subsistence harvesting of mammals, birds, invertebrates, and fish provides nutritional support for many indigenous communities and important socio-cultural activity throughout the Circumpolar North.[2,3] Furthermore, salmon fisheries in Alaska are among the most productive in the world, providing escapement of approximately 74.3 million (all species) in 2020 and attracting sport-fishing tourism worldwide.[4]

6PPD-quinone (CAS no. 2754428-18-5, 6PPDQ, Figure 1) has very recently gained international recognition due to its

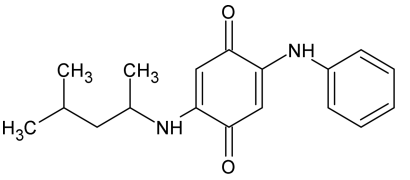

Figure 1. Structure of 6PPD-quinone (6PPDQ).

Received: July 18, 2023
Revised: October 31, 2023
Accepted: November 1, 2023
Published: November 30, 2023

© 2023 American Chemical Society

extreme toxicity to Pacific salmon (coho LC_{50} = 95 ng/L).[5] 6PPDQ is the transformation product of the antiozonant 6-PPD, a ubiquitous compound found in tire rubber.[6] The compound has been detected across coho salmon-bearing urban waterways on the west coast[5] and very recently in Anchorage stormwater runoff.[7] Recent work has reported 6PPDQ to be stable against thermal and photochemical degradation in tire particles over a 72 h period; however, the aqueous photochemical pathways predominant in natural systems have not been investigated to date.[8] With the rapid emergence of this aquatic contaminant, it is essential to understand the compound's fate in the Alaskan environment, which supports the world's largest stocks of wild Pacific salmon.[9]

High latitude regions experience extreme seasonal fluctuations in photoperiods compared to those at lower latitudes. For contaminants that are sensitive to photodegradation, this factor, which is also accompanied by low temperatures in winter months, is frequently cited as an environmental driver of persistence.[10−13] Thus, the timing and magnitude of aquatic photochemical processing in high latitudes can lead to differences in the observed attenuation rates of aquatic contaminants compared to temperate regions. Broadly, there are two primary pathways, direct and indirect, by which aquatic contaminants are photochemically degraded in the environment. Direct photodegradation requires absorption of a photon by a compound to induce chemical breakdown, which may also include intersystem crossing to triplet excitation states prior to decomposition. Indirect photodegradation includes a variety of decomposition pathways in which the compound of interest reacts with photon-induced reactive transient species. These reactive species include hydroxyl radical ($^{\bullet}OH$), singlet oxygen ($^1O_2$), and triplet-state chromophoric dissolved organic matter ($^3CDOM^*$). As these factors vary across surface waters, degradation kinetics can be site-specific, and therefore, it is difficult to predict if the primary pathways by which a contaminant degrades are unknown.

The overall goal of this work is to assess the fundamental photochemical pathways by which 6PPDQ degrades at high latitudes and to detect and identify the primary photoproducts formed. This was accomplished by illuminating solutions containing 6PPDQ and select reactive species quenchers and sensitizers under simulated high-latitude conditions at 4, 12, and 20 °C to determine the contribution of indirect processes involving $^{\bullet}OH$, $^1O_2$, and $^3CDOM^*$ to the attenuation of 6PPDQ.

2. MATERIALS AND METHODS

2.1. Chemical Reagents. 6PPDQ (>98%) and the deuterated internal standard D5-6PPDQ (>98%) were purchased from HPC Standards, Inc. (Atlanta, GA). 6PPDQ used during preliminary LC-MS/MS method development was synthesized by the Pirrung laboratory group at UC Riverside. Formic acid (Optima for LC-MS), methanol (Optima for LC-MS), and sodium azide (>99%) were purchased from Fisher Scientific (Waltham, MA). Water (LC-MS grade), acetonitrile (LC-MS grade), isopropanol (LC-MS grade), sodium molybdate dihydrate (ACS grade), cesium chloride (>99.9%), sodium borate decahydrate (ACS Reagent grade), and furfuryl alcohol (98%) were obtained from VWR (Radnor, PA). 2-Nitrobenzaldehyde (2NB, >99%) was purchased from Alfa Aesar (Tewksbury, MA). Suwanee River fulvic acid was obtained from the International Humic Substances Society (Denver, CO). The laboratory's liquid argon supply was sourced from AirGas (Radnor, PA). Deuterium oxide (99.8%) was purchased from Acros Organics, now Thermo Scientific Chemicals (Waltham, MA). Potassium nitrate (>99%), benzene (>99.9%), and phenol (PESTANAL, analytical standard) were purchased from Sigma-Aldrich (St. Louis, MO). Hydrogen peroxide solution (Veritas Low Trace Metal, 30%, w/w) was purchased from GFS Chemicals (Columbus, OH). 2,3,6-Trimethylphenol (>98%) was purchased from TCI Chemicals (Tokyo, Japan).

2.2. Molar Absorptivity. The molar absorptivity of 6PPDQ ($\varepsilon_{6PPDQ,\lambda}$; M^{-1} cm^{-1}) was determined via high-performance liquid chromatography with diode array detection due to the limited quantity of available 6PPDQ standard solution. Similar methods for the calculation of molar absorptivity have been reported.[14,15] Briefly, solutions containing 340, 50, 25, or 10 μM 6PPDQ were prepared in methanol and water (80:20, v/v). Each solution was injected (10 μL) onto an InfinityLab Poroshell 120 EC-C18 column (3.0 × 50 mm; 2.7 μm) and eluted isocratically with methanol and water (80:20, v/v). The retention time of 6PPDQ was 1.307 min. Absorbance spectra were recorded between 205 and 800 nm at 1 nm increments. Blank spectra were subtracted from each 6PPDQ spectrum prior to baseline correction. Peak areas for each wavelength ($area_\lambda$; mAU·s) were calculated from absorbance and the measured peak area at 360 nm using eq 1

$$\text{area}_\lambda = A_\lambda \cdot \Delta t \cdot \frac{A_{360} \cdot \Delta t}{\text{measured peak area for 360 nm}} \quad (1)$$

where A_λ is the absorbance (mAU) at wavelength λ (nm) and Δt is the chromatographic peak width (s). Molar absorptivity was then calculated as the slope of the line obtained by plotting eq 2

$$\text{area}_\lambda = \varepsilon_\lambda \cdot \frac{b \cdot N \cdot 6 \times 10^{-7}}{F} \quad (2)$$

where b is the path length (cm), N is the moles of 6PPDQ injected, F is the flow rate (mL min^{-1}), and the factor 6×10^{-7} is for the unit conversion of seconds to minutes, mAU to AU, and mL to L. HPLC-DAD molar absorptivity calculations were validated by using caffeine prior to 6PPDQ measurements (Figure S1).

2.3. Degradation Experiments. All microcosms (n = 4/treatment) contained 50 ppb (~168 nM) of 6PPDQ and were prepared in a mixture of water and acetonitrile (80:20, v/v; 5.1:1 w/w) in order to prevent sorption to glassware observed during preliminary experiments (data not shown). Additional microcosms (n = 4) were prepared containing select sensitizing and quenching agents. Treatments selected for pathway sensitization included 1 mM potassium nitrate (KNO_3) to generate $^{\bullet}OH$, 100 mM cesium chloride (CsCl) to promote intersystem crossing and assess triplet state 6PPDQ reactivity, and 10 mg L^{-1} Suwannee River fulvic acid (SRFA) as a model for evaluating the impacts of $^3CDOM^*$ on 6PPDQ attenuation. Treatments selected for pathway inhibition included 10 mg L^{-1} SRFA with the addition of either 17.5 mM isopropanol (IPA), 5 mM furfuryl alcohol (FFA), or 1 mM trimethylphenol (TMP) to selectively quench $^{\bullet}OH$, $^1O_2$, and $^3CDOM^*$, respectively. All microcosms were incubated under simulated solar conditions typical of Southcentral Alaska summers (250 W m^{-2}),[16−19] using a SunTest XLS+ with a

https://doi.org/10.1021/acs.est.3c05742
Environ. Sci. Technol. 2023, 57, 20813−20821

suncool attachment for air temperature regulation (Atlas Materials, Mount Prospect, IL). Experiments were conducted first at 20 °C in quartz test tubes and then repeated at 4 and 12 °C in water cooled jacketed beakers covered with a saran wrap film. Jacketed beakers were not used for the 20 °C experiments due to the formation of condensation on the inside of the beaker covers during preliminary experiments. 2-Nitrobenzaldehyde (2NB) actinometry was performed to account for positional and interday variations of the solar simulator light intensity. SunTest XLS+ emission spectrum, 2NB actinometry corrections, and 2NB analysis were reported previously.[19] 2NB rate constants used for the calculation of positional correction factors for the jacketed beakers in this work are available in the Supporting Information (Figure S2).

Supplementary microcosms were prepared containing SRFA with sodium azide (1 mM, NaN_3, $n = 3$) to quench $^1O_2$, SRFA in deuterium oxide (D_2O, $n = 3$) to increase $^1O_2$ reactivity by reducing its relaxation rate in solution, in Ar-purged water and ACN to reduce triplet quenching by molecular oxygen, or in molybdate (MoO_4^{2-}) and hydrogen peroxide (H_2O_2) at pH 10 to thermally generate $^1O_2$ and selectively assess its contribution toward 6PPDQ degradation, as described previously.[19,20] Supplemental microcosms were incubated at 20 °C; MoO_4^{2-}/H_2O_2 microcosms, MoO_4^{2-} controls, H_2O_2 controls, and pH 10 controls were incubated in the dark. Additional microcosms contained natural waters collected from Lower Fire Lake (61.351868, −149.546737), Anderson Lake (61.620726, −149.335903), and Kings Lake (61.618322, −149.358120) by the Alaska Department of Fish and Game. Lake waters were stored frozen (−20 °C) in the dark and were filtered (0.22 μm) immediately prior to use. Freezing, as a preservation technique, is acknowledged in Fellman et al.[21] Lake water parameters, including dissolved ion concentrations, pH, dissolved organic carbon concentration, UV/visible light absorbance, and light screening factors (S_λ), are provided in the Supporting Information (section S1, Table S1, and Figure S3). Lake water microcosms were illuminated at 20 °C only due to the limited quantities available for this work, while 18 MΩ cm water microcosms were illuminated at all temperatures.

All microcosms were subsampled (100 μL) after 0, 1, 4, 8, 24, and 48 h while dark controls ($n = 3$) for each treatment were subsampled at the start and end of each experiment; average 6PPDQ loss in dark controls was <10% across all experiments. At each time point, samples from each microcosm were quenched with a 55.5 mM solution of FFA in IPA containing the deuterated internal standard (D5-6PPDQ, final concentration 25 ppb) prior to analysis via liquid chromatography tandem triple quadrupole mass spectrometry (LC-MS/MS, Section S2a).

Calculations for illumination-position-corrected first-order rate constants (j), half-lives ($t_{1/2}$), and apparent quantum yields (ϕ) for the photochemical degradation of 6PPDQ by simulated sunlight were previously described.[18] Briefly, j (h^{-1}) were calculated from eq 3

$$\frac{\ln(C_t/C_0)}{F_P} = jt \tag{3}$$

where C_0 and C_t are the concentration (ppb) of 6PPDQ at time t (h), respectively, and F_P is the illumination correction factor calculated via 2NB actinometry. Corrected rate constants were then used to calculate $t_{1/2}$ (h) and ϕ with eqs 4 and 5

$$t_{1/2} = \frac{\ln(2)}{j} \tag{4}$$

$$\phi = \frac{j_{6PPDQ}}{j_{2NB}} \cdot \frac{\sum_\lambda (\varepsilon_{2NB,\lambda} \cdot I_\lambda)}{\sum_\lambda (\varepsilon_{6PPDQ,\lambda} \cdot I_\lambda)} \cdot \phi_{2NB} \tag{5}$$

where j, I_λ, and ε_λ are the illumination corrected first-order rate constants (s^{-1}) volume-averaged photon flux (mol photons L^{-1} s^{-1}) at wavelength λ (nm) and molar absorptivity (M^{-1} cm^{-1}). Rate constants, half-lives, and apparent quantum yields are presented as the average ± standard deviation ($n = 4$). Reported statistical differences were determined via analysis of variance (ANOVA) with posthoc Tukey honest significant difference (HSD) comparisons using JMP Pro 16 (SAS Institute, Cary, NC) ($\alpha = 0.05$). The Wilk-Shapiro test ($W > 0.9$) was performed to confirm normally distributed residual error.

2.4. Nontarget Photoproduct Identification. Experiments for microcosms containing KNO_3, SRFA, and SRFA with TMP at 12 °C along with MoO_4^{2-} with H_2O_2 at 20 °C were repeated ($n = 4$), and the entire volume (15 mL) was concentrated via Hydrophilic-Lipophilic-Balance (HLB, Waters) solid phase extraction (SPE) after 0 h or approximately four half-lives to identify 6PPDQ photoproducts. These treatments were selected on the basis of the results from initial degradation experiments outlined in section 2.3 and discussed in sections 3.1 and 3.2; briefly, these treatments provide representative photoproducts for the direct and indirect photochemical degradation of 6PPDQ via pathways including $^•OH$, $^1O_2$, and the phenoxy radical discussed below. Photoproducts of 6PPDQ degradation were identified in extracts using ultra-high-performance liquid chromatography with high-resolution Orbitrap mass spectrometry (UHPLC-Orbitrap). Methods for SPE and UHPLC-Orbitrap analysis are available in the Supporting Information (section S2b).

3. RESULTS AND DISCUSSION

3.1. Molar Absorptivity and Direct Photochemical Degradation. Tabulated molar absorptivities and first-order rate constants for 6PPDQ for all treatments are available in the Supporting Information (Tables S3 and S4). 6PPDQ strongly absorbs light within the solar spectrum with a prominent local absorbance maximum at 357 nm (ε = 22,363 M^{-1} cm^{-1}) and a weak absorbance tail extending to approximately 665 nm (Figure 2a and Table S3); to our knowledge, this work is the first to calculate molar absorptivities for 6PPDQ. Based upon the strong light absorbance of 6PPDQ, it was anticipated that direct photochemical degradation would be a significant contributor to its environmental attenuation. However, the direct aqueous photodegradation of 6PPDQ was slow and observed to decrease with decreasing temperature from a half-life of 17.4 ± 4.5 h (j = 0.042 ± 0.009 h^{-1}) at 20 °C to no observable degradation over the 48 h period at 4 °C or in the dark controls (Figure 2b). No observable degradation in the dark controls is consistent with previously reported half-lives for 6PPDQ hydrolysis (12.8−16.3 d).[22] Apparent quantum yields for the aqueous photochemical degradation of 6PPDQ were $1.1 \times 10^{-5} \pm 3.4 \times 10^{-6}$ and $1.5 \times 10^{-5} \pm 4.3 \times 10^{-6}$ at 12 and 20 °C, respectively. The observed temperature

https://doi.org/10.1021/acs.est.3c05742
Environ. Sci. Technol. 2023, 57, 20813−20821

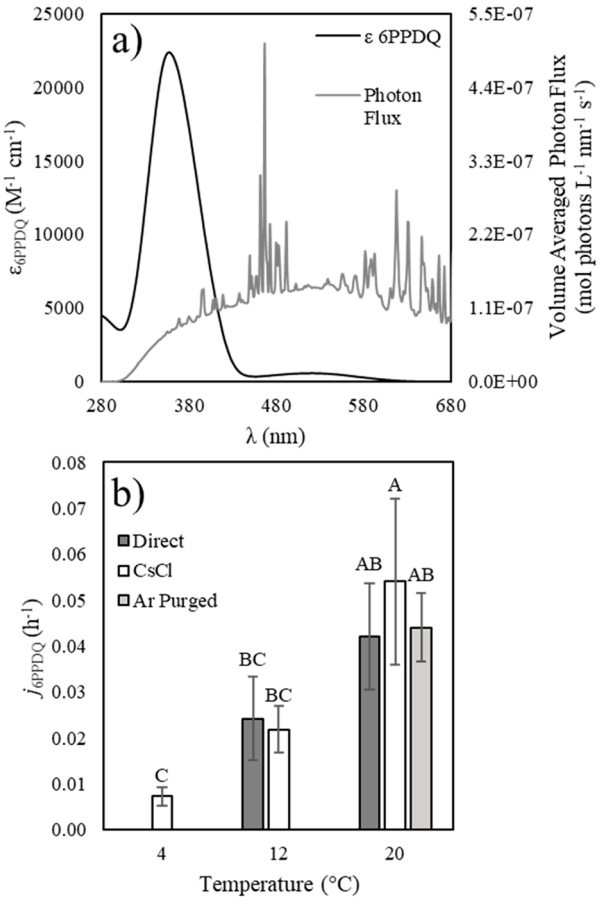

Figure 2. (a) Molar absorptivity (ε, M^{-1} cm^{-1}) of 6PPDQ and volume-averaged photon flux (mol photons L^{-1} nm^{-1} s^{-1}) for the SunTest XLS+ solar simulator. (b) Average pseudo-first-order rate constants (j, h^{-1}, n = 4) for the direct (dark gray bars) and triplet-sensitized (0.1 M CsCl and Ar purged, open, and light gray bars, respectively) photochemical degradation of 6PPDQ at 4, 12, and 20 °C. Error bars represent one standard deviation. Rate constants that do not share a letter label (A−C) are significantly different ($p < 0.05$, Tukey HSD).

dependence of the direct photochemical degradation of 6PPDQ may be due to increased internal conversion efficiency at lower temperatures, resulting in the dissipation of absorbed energy through vibrational and rotational relaxation, or the formation of a quinone−water exciplex as previously observed for *p*-benzoquinone.[23] The addition of 100 mM Cs^+ to promote intersystem crossing of excited singlet to triplet state 6PPDQ was not observed to have a significant effect (α = 0.05) at 12 and 20 °C; however, slow degradation of 6PPDQ ($t_{1/2}$ = 100.6 ± 29.6 h, j = 0.007 ± 0.002 h^{-1}) was observable at 4 °C. This slight enhancement of degradation at 4 °C in the presence of the triplet sensitizer is likely attributable to the inverse relationship of triplet-state lifetimes and temperature. This is consistent with previous work showing that triplet-state decay rates, through intersystem crossing or secondary quenching, can decrease with decreasing temperature.[24−26] Direct photochemical degradation experiments conducted using Ar-purged water at 20 °C showed no change relative to that of oxygenated water, supporting the conclusion that 6PPDQ does not directly degrade through a triplet excitation pathway. Activation energies for the direct photochemical degradation of 6PPDQ are available in the Supporting Information (Figure S4). Of equal importance is the observation that 6PPDQ degradation was not reduced by Ar purging, suggesting that self-sensitization (i.e., reaction with $^1O_2$ produced via quenching of triplet 6PPDQ by molecular oxygen) was not significant. While self-sensitization has been observed for many quinones, including *p*-benzoquinone, it may be that internal conversion of absorbed photon energy is more efficient in the larger and less rigid structure of 6PPDQ which reduces the overall production or reactivity of its triplet state.[27]

3.2. Indirect Photochemical Pathways. Indirect photochemical processes involving the reactive oxygen species $^{\bullet}OH$ and $^1O_2$ were observed to be significant pathways for the degradation of aqueous 6PPDQ at all of the studied temperatures (Figure 3a). Half-lives for 6PPDQ ranged from 6.1 ± 1.7 h (j = 0.120 ± 0.030 h^{-1}) at 4 °C to 2.6 ± 0.1 h (j = 0.272 ± 0.013 h^{-1}) at 20 °C in the presence of 1.0 mM potassium nitrate, a $^{\bullet}OH$ sensitizer, and 5.2 ± 0.8 h (j = 0.135 ± 0.019 h^{-1}) at 4 °C to 11.2 ± 0.9 h (j = 0.062 ± 0.005 h^{-1}) at 20 °C in the presence of 10 mg L^{-1} Suwannee River fulvic acid (SRFA), a $^{\bullet}OH$ and $^1O_2$ sensitizer. The inverse relationship of 6PPDQ half-lives in the presence of SRFA with temperature is consistent with the decreased production of reactive oxygen species by triplet-dissolved organic matter resulting from the decrease in triplet state lifetimes at higher temperatures.[24−26] It was originally hypothesized that TMP would decrease the observed rate of 6PPDQ degradation by quenching triplet SRFA. Interestingly, 6PPDQ degradation was accelerated when trimethylphenol (TMP, 1 mM) was added as a triplet scavenger in SRFA microcosms ($t_{1/2}$ = 4.0 ± 0.2 h, j = 0.176 ± 0.010 h^{-1} at 20 °C; Figure 3a). It is possible that 6PPDQ reacts with the phenoxy radical that has been proposed as the initial product following electron transfer between TMP and triplet-dissolved organic matter.[28] This observation is also consistent with previous work in which electron-poor phenols, such as TMP, were observed to form phenoxy radicals via one-electron oxidation by model triplet sensitizers and CDOM that react with electron-rich aquatic contaminants. It has been hypothesized that these phenoxy radicals comprise a pool of long-lived photooxidants (LLPOs) in DOM that significantly contribute to the degradation of electron-rich aquatic contaminants, such as phenols, anilines, and now quinones.[29] Formation of the phenoxy radical may also explain the dramatic increase in the degradation of 6PPDQ at 4 and 12 °C ($t_{1/2}$ = 0.68 ± 0.03 h and 0.74 ± 0.04 h, j = 1.02 ± 0.04 h^{-1} and 0.943 ± 0.050 h^{-1}, respectively; Figure 3a) as lifetimes for both SRFA triplet states and the phenoxy radical could be expected to increase with decreasing temperature, thereby increasing the production of the phenoxy radical and the probability that it react with 6PPDQ in solution;[30] this merits further investigation into the interaction of phenoxy radical formation and 6PPDQ.

To further investigate the reaction of 6PPDQ with $^1O_2$, molybdate (1 mM) and hydrogen peroxide (3 mM) were used to generate $^1O_2$ in the dark. 6PPDQ rapidly degraded in this system ($t_{1/2}$ = 0.055 ± 0.004 h, j = 12.6 ± 0.9 h^{-1}) (Figure 3b), and no degradation was observed in hydrolysis controls (pH 10) or molybdate controls; however, equivalent rapid degradation was observed in the hydrogen peroxide only controls. We repeated these experiments with the addition of ethylenediaminetetraacetic acid (EDTA) to eliminate the possibility of metal-induced generation of $^{\bullet}OH$ and found identical results. While $^1O_2$ production was confirmed in this system with FFA ($[^1O_2]_{ss}$ = 2 pM) and may have contributed

https://doi.org/10.1021/acs.est.3c05742
Environ. Sci. Technol. 2023, 57, 20813−20821

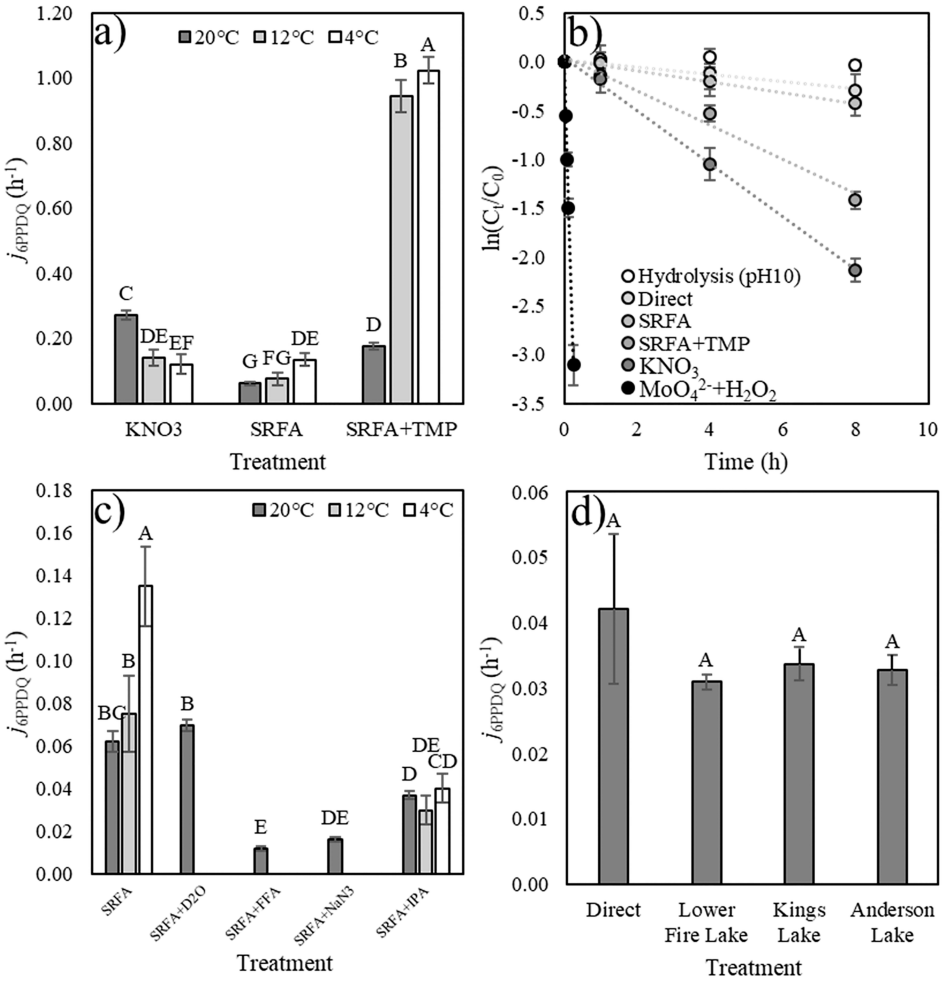

Figure 3. (a) Average pseudo-first-order rate constants (j, h^{-1}, n = 4) for the photochemical degradation of 6PPDQ in microcosms containing potassium nitrate (KNO_3, 1.0 mM), Suwannee River fulvic acid (SRFA, 10 mg L^{-1}), or SRFA with trimethyl phenol (TMP, 1 mM) at 4, 12, and 20 °C; n = 2 for SRFA+TMP at 4 and 12 °C due to rapid degradation preventing 6PPDQ detection after 8 h. (b) Natural log transformed first-order kinetics plots for the degradation of 6PPDQ at 20 °C. (c) Average pseudo-first-order rate constants (j, h^{-1}, n = 4) for the photochemical degradation of 6PPDQ in microcosms containing SRFA, SRFA with isopropanol (IPA, 17.5 mM), or SRFA with furfuryl alcohol (FFA, 5 mM) at 4, 12, and 20 °C, as well as SRFA in D_2O or SRFA with sodium azide (NaN_3, 1 mM) at 20 °C. (d) Average pseudo-first-order rate constants (j, h^{-1}, n = 4) for the photochemical degradation of 6PPDQ in pure water (direct) and natural lake waters. Error bars represent one standard deviation. Rate constants within each plot that do not share a letter label (A−G) are significantly different (p < 0.05, Tukey HSD).

to the degradation of 6PPDQ, it is apparent that there is a second unknown reaction contributing to 6PPDQ attenuation in these microcosms. Previous work has reported that semiquinones, produced by the one-electron reduction of quinones, may catalyze metal-independent reduction of hydrogen peroxide to generate a hydroxyl radical.[31−33] While this work focuses on photochemical pathways, future work should investigate the potential interplay between 6PPDQ redox properties and environmental photoproduction of hydrogen peroxide.[34] To further test the hypothesis that the production of $^1O_2$ in sunlit waters by dissolved organic matter may contribute to its degradation in the environment, we conducted additional experiments employing either furfuryl alcohol (FFA, 5 mM) or sodium azide (NaN_3, 1 mM) as a $^1O_2$ scavenger in SRFA microcosms. The attenuation rate of 6PPDQ in the presence of $^1O_2$ scavengers was observed to decrease more than in the presence of the $^{\bullet}$OH scavenger isopropanol (IPA, 17.5 mM) (Figure 3c). Observation of no degradation in microcosms containing FFA at 4 and 12 °C may have been due to the compound effects of the quencher, light screening by SRFA (S_{369} = 0.907, Figure S3 and as previously described[19]), and consumption of dissolved oxygen by FFA over the course of the experiment. Furthermore, the photochemical degradation of 6PPDQ in SRFA was only slightly enhanced when repeated in D_2O ($t_{1/2}$ = 9.9 ± 0.4 h, j = 0.070 ± 0.003 h versus ($t_{1/2}$ = 11.2 ± 0.9 h, j = 0.062 ± 0.005 h^{-1}). Taken together, $^1O_2$ does not appear to contribute significantly to the overall photochemical degradation of 6PPDQ; however, the presence of photochemically induced radical oxygen species, e.g., $^{\bullet}$OH, and potentially other CDOM-derived phenoxy radicals, are suggested to cause rapid 6PPDQ degradation under environmental conditions of cool sunlit waters typical of high-latitude environments.

The degradation of 6PPDQ in natural lake waters was investigated. Lake water parameters are provided in the Supporting Information (section S1, Table S1, Figure S3). Our results showed that degradation rates in natural waters were not significantly different from the direct photochemical degradation of 6PPDQ at 20 °C, with half-lives ranging from 20.6 ± 1.5 h (j = 0.034 ± 0.003 h^{-1}) to 22.4 ± 0.84 h (j =

https://doi.org/10.1021/acs.est.3c05742
Environ. Sci. Technol. 2023, 57, 20813−20821

0.031 ± 0.001 h^{-1}) for the three studied lake waters (Figure 3d). Correcting for light screening by CDOM (S_λ, Figure S3) did not significantly alter the measured half-lives due to minimal absorption at the wavelength where the rate of 6PPDQ light absorption is maximized (S_{369} = 0.973−0.978, Figure S3). Furthermore, the lake waters available for this work were low in nitrate (37.6−77.6 μM) and dissolved organic matter (4.40−4.44 mg L^{-1}) with $SUVA_{254}$ ranging from 1.41−2.19 L mg^{-1} m^{-1}, indicating that these waters were not photochemically reactive compared to the SRFA solution used in this work (S_{369} = 0.907, $SUVA_{254}$ = 4.78 L mg^{-1} m^{-1}). As a result, the rate of •OH production (section S3, Table S5), used as the primary measurement of photochemical reactivity based on the minimal contribution of $^1O_2$ to 6PPDQ degradation, was low in the natural lake waters relative to the SRFA solution at 20 °C. The low production of •OH may have been exacerbated by the use of 20% ACN, necessary to prevent sorption of 6PPDQ, as ACN is known to reduce the reactivity of •OH.[35,36] Based on this, the molar absorptivity and apparent quantum yield determined in this work were used to calculate the action spectra for 6PPDQ under the TUV-modeled solar photon flux for Anchorage, AK, at midday of the summer solstice (Figure 4).[37] The calculated half-life for 6PPDQ under

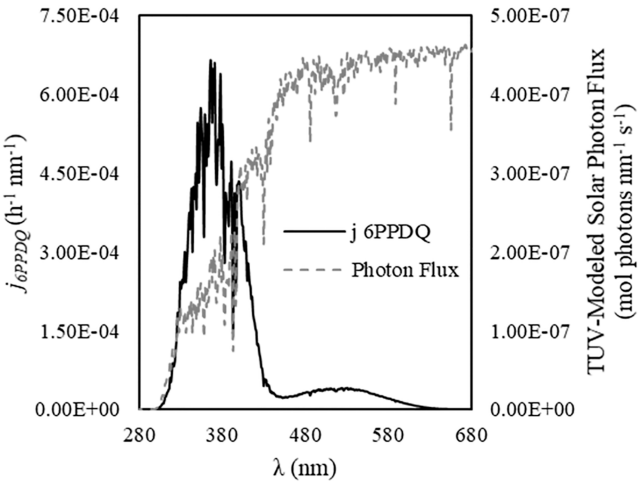

Figure 4. Action spectra for the photochemical degradation of 6PPDQ under TUV-modeled solar photon flux for Anchorage, AK, at the midday of the summer solstice.

the modeled conditions (21.9 h) was in good agreement with the experimental results (20.6−22.4 h). To clarify, the calculated half-life represents the peak attenuation rate for 6PPDQ under the most conservatively modeled photochemical conditions and does not necessarily reflect the environmental degradation half-life that will be observed. The environmentally observed half-life will be influenced by the depth and clarity of the waterbody, the zenith angle, and the rate of reactive oxygen species production by CDOM. Furthermore, the quantum yields for 6PPDQ presented in this work represent apparent quantum yields under the simulated solar conditions of the photochamber. While minor, the secondary peak in the molar absorptivity (Figure 2a) and action spectrum (Figure 4) indicate that the quantum yield for the degradation of 6PPDQ may have a slight wavelength dependence, which may have compounding effects with CDOM light attenuation at specific wavelengths in the environment. Future work relating the optical and molecular-level characterization of CDOM with respect to the photochemical production of reactive species is required to explain the impact this interplay will have on the environmental persistence of 6PPDQ.

3.3. Photoproducts and Proposed Degradation Pathways. We characterized transformation products that resulted from the predominant photochemical pathways identified in this study, which are indirect processes involving radicals. Repeat experiments were performed with water containing either KNO_3, SRFA, SRFA+TMP, or MoO_4^{2-}+H_2O_2. Subsamples were collected after approximately four half-lives. To facilitate analysis of transformation products using UHPLC-Orbitrap, samples were preconcentrated using SPE (HLB, Waters, section S2). Proposed transformation product details, including retention time, molecular formula, mass error, and fragmentation, are provided in the Supporting Information (Table S6). Structures are proposed with Level 3 and 4 confidence, according to the framework established by Schymanski et al. Briefly, the proposed products are tentative candidates with unambiguous molecular formula (Level 4) with fragmentation data (Level 3) but insufficient evidence to propose an exact structure.[38] In particular, this is due to the existence of positional isomers, as observed by the occurrence of identical molecular formulas at multiple retention times (Table S6). For this study, this level of confidence is sufficient to propose pathways when integrated with our understanding of the photochemical pathways presented above. Overall, nontarget analyses revealed 26 molecular formulas consistent with the transformation of 6PPDQ through four processes: (1) oxidative decomposition of the quinone ring, (2) deamination following rearrangement of side-chain groups, (3) dealkylation, and (4) reduction (Figure 5). The majority of transformation products were consistent with highly oxidized quinone ring-opening products, which is consistent with previous observations of 6PPDQ transformation in the presence of ozone.[39] Considering previous mechanistic insight from Rossomme et al, who assessed 6PPD transformation to 6PPDQ,[40] we believe the central quinone ring system of 6PPDQ is rapidly oxidized by pathways exclusive of ozone, such as aqueous reactive oxygen species. Interestingly, an unknown $C_{21}H_{26}N_2O_5$ transformation product was detected in both positive and negative mode. This molecular formula is consistent with an isopropyl alcohol adduct of a 6PPDQ oxidation product, which occurred when the reaction was quenched (Figure 5, Table S6). We hypothesize that the oxidized quinone ring, also observed by Seiwert et al., efficiently traps radical electrons that are further oxidized into the ring opening products.[39]

Dealkylation of the amine side chains was also observed. This process is consistent with prior studies that identified ozone-mediated transformation of 6PPDQ;[39] however, to our knowledge the remaining two processes, rearrangement and reduction, have not been previously reported for 6PPDQ. Transformation products for these processes were only detected after reaction with radical species in this work (Figure 5, KNO_3 and SRFA+TMP microcosms), which could explain their absence in previous work investigating the ozonation of 6PPDQ. Rearrangement products are exclusive to radical-sensitized processes (Figure 5, gold pathway); this suggests that hydrogen abstraction from a side chain facilitates migration of the phenyl or diisopropyl group to the quinone oxygen prior to photochemical deamination.

https://doi.org/10.1021/acs.est.3c05742
Environ. Sci. Technol. 2023, 57, 20813−20821

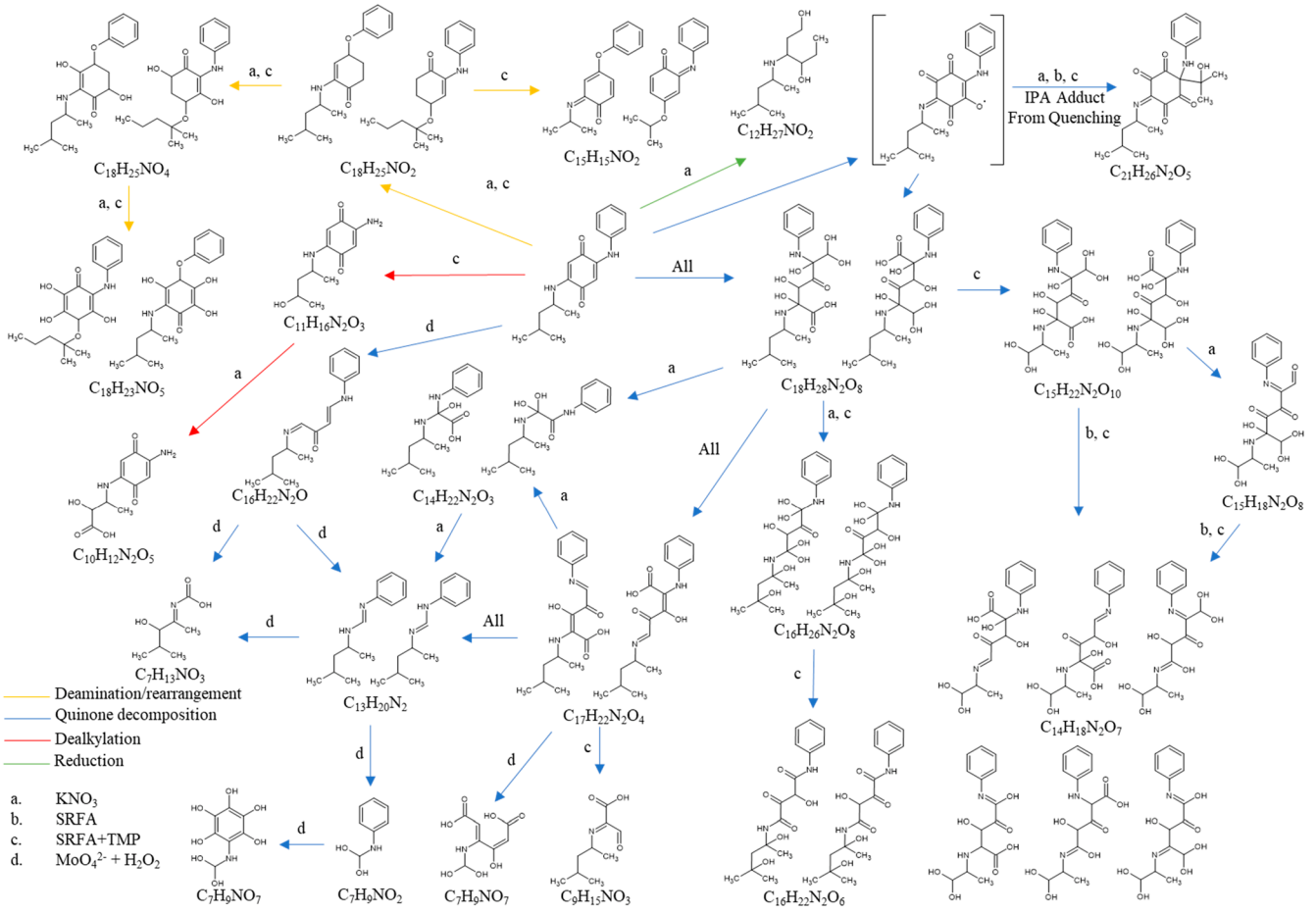

Figure 5. Proposed pathways for 6PPDQ transformation in (a) KNO_3, (b) SRFA, (c) SRFA+TMP, and (d) MoO_4^{2-}+H_2O_2 containing microcosms include quinone decomposition (blue), rearrangement and deamination (gold), dealkylation (red), and reduction (green). Provided structures for 6PPDQ transformation products have been proposed based upon calculated molecular formulae and fragmentation spectra, where available. Possible isomeric structures are presented, though they do not represent an exhaustive list of possibilities.

In summary, this work identified that temperature-dependent generation of reactive oxygen species by CDOM accelerates the photodegradation of 6PPDQ in high latitude waters via oxidation and cleavage of the central quinone ring. While additional work is required to confirm the specific mechanisms by which these proposed transformations occur, these processes are consistent with a recent review of advanced oxidation pathways. This also shows how radical-initiated ring opening, dealkylation, and deamination reactions could be significant contributors to the transformation of 6PPDQ, consistent with studies on other amine-containing compounds.[41]

4. ENVIRONMENTAL IMPLICATIONS

This study shows that the primary pathways by which 6PPDQ is expected to degrade photochemically are temperature dependent and modulated by the presence and reactivity of DOM. Specifically, direct photochemical processes will dominate in warm waters (20 °C), and under these conditions, DOM is anticipated to inhibit the attenuation of 6PPDQ through light-screening processes. In cool sunlit waters (4−12 °C), indirect processes are expected to significantly contribute to the overall degradation mechanism, involving DOM-mediated production of radical oxygen species, such as hydroxyl and phenoxy radicals. However, the use of acetonitrile (20%), a commonly used cosolvent to limit sorption to container walls in similar types of studies, may induce an underestimation of indirect processes as acetonitrile is known to react with hydroxyl radical.[35,36,42−44] Nevertheless, measurement of hydroxyl radical formation rates and water quality parameters supports the observed differences between the degradation of 6PPDQ in natural waters and SRFA solutions and enables extension of these results to other environmental systems. Furthermore, investigation of covarying pH, dissolved oxygen, and temperature on 6PPDQ degradation and the formation of LLPOs is a priority direction for future work. Finally, transformation product screening via UHPLC-Orbitrap mass spectrometry revealed molecular formulae consistent with four pathways: oxidation of the quinone ring, deamination, dealkylation, and reduction. Tentative products are proposed based upon these formulae to aid future nontarget studies monitoring the degradation of this emerging contaminant in diverse aquatic systems.

■ ASSOCIATED CONTENT

Supporting Information

The Supporting Information is available free of charge at https://pubs.acs.org/doi/10.1021/acs.est.3c05742.

HPLC-DAD molar absorptivity validation. 2NB actinometry flux mapping. Surface water characterization.

https://doi.org/10.1021/acs.est.3c05742
Environ. Sci. Technol. 2023, 57, 20813−20821

Description of LC-MS/MS quantitative analysis and acquisition parameters. Description of solid-phase extraction and UHPLC-Orbitrap nontarget analysis. Tabulated molar absorptivity of 6PPDQ. Tabulated rate constants for the degradation of 6PPDQ in experimental treatments. Solution absorbance and light screening factors for lake water and SRFA solutions. Arrhenius plots for the degradation of 6PPDQ in direct, CsCl and KNO_3 microcosms. Hydroxyl radical formation rates. Tabulated 6PDDQ transformation products identified via UHPLC-Orbitrap (PDF)

AUTHOR INFORMATION

Corresponding Author

Zachary C. Redman − *Department of Chemistry, College of Arts and Sciences, University of Alaska Anchorage, Anchorage, Alaska 99508, United States;* orcid.org/0000-0002-4158-524X; Email: zcredman@alaska.edu

Authors

Jessica L. Begley − *Department of Chemistry, College of Arts and Sciences, University of Alaska Anchorage, Anchorage, Alaska 99508, United States*

Isabel Hillestad − *Department of Chemistry, College of Arts and Sciences, University of Alaska Anchorage, Anchorage, Alaska 99508, United States*

Brian P. DiMento − *Department of Chemistry, College of Arts and Sciences, University of Alaska Anchorage, Anchorage, Alaska 99508, United States*

Ryan S. Stanton − *Department of Chemistry, University of California, Riverside, California 92521, United States*

Alon R. Aguaa − *Department of Chemistry, University of California, Riverside, California 92521, United States*

Michael C. Pirrung − *Department of Chemistry, University of California, Riverside, California 92521, United States*

Patrick L. Tomco − *Department of Chemistry, College of Arts and Sciences, University of Alaska Anchorage, Anchorage, Alaska 99508, United States*

Complete contact information is available at: https://pubs.acs.org/10.1021/acs.est.3c05742

Funding

Research reported in this publication was supported by the National Science Foundation awards 2203761 and 2019123

Notes

The authors declare no competing financial interest.

ACKNOWLEDGMENTS

We thank J. Torres for their assistance during initial development of SPE and LC-MS/MS methods for 6PPDQ analysis. We thank N. Smith and A. Pavia for their assistance with day to day laboratory tasks and L. Weiland for performing ion chromatography and dissolved organic carbon measurements. Additional thanks to K. Dunker, B. Parker, and C. Jacobson from the Alaska Department of Fish and Game for collecting and providing regional lake water samples.

REFERENCES

(1) Schindler, D. W.; Smol, J. P. Cumulative effects of climate warming and other human activities on freshwaters of Arctic and Subarctic North America. *Ambio* **2006**, *35*, 160−168.

(2) Holen, D. Fishing for community and culture: the value of fisheries in rural Alaska. *Polar Record* **2014**, *50* (4), 403−413.

(3) Krieg, T. M.; Lemons, T.; Welch, C. An Overview of the Subsistence Fisheries of the Bristol Bay Area, 2015. Available from: https://www.adfg.alaska.gov/static/regulations/regprocess/fisheriesboard/pdfs/2015-2016/bristolbay/SP2_SP2015-004.pdf.

(4) Brenner, R.; Munro, A. R.; Larson, S. J.; Carroll, A. M. *Run forecasts and harvest projections for 2021 Alaska salmon fisheries and review of the 2020 season*; Alaska Department of Fish and Game, Division of Sport Fish, Research and Technical Services, 2021.

(5) Tian, Z.; Zhao, H.; Peter, K. T.; Gonzalez, M.; Wetzel, J.; Wu, C.; Hu, X.; Prat, J.; Mudrock, E.; Hettinger, R.; Cortine, A. E.; Biswas, R. G.; Kock, F. V. C.; Soong, R.; Jenne, A.; Du, B.; Hou, F.; He, H.; Lundeen, R.; Gilbreath, A.; Sutton, R.; Scholz, N. L.; Davis, J. W.; Dodd, M. C.; Simpson, A.; McIntyre, J. K.; Kolodziej, E. P. A ubiquitous tire rubber−derived chemical induces acute mortality in coho salmon. *Science* **2021**, *371* (6525), 185−189.

(6) Zhao, H. N.; Hu, X.; Tian, Z.; Gonzalez, M.; Rideout, C. A.; Peter, K. T.; Dodd, M. C.; Kolodziej, E. P. Transformation Products of Tire Rubber Antioxidant 6PPD in Heterogeneous Gas-Phase Ozonation: Identification and Environmental Occurrence. *Environ. Sci. Technol.* **2023**, *57* (14), 5621−5632.

(7) Anchorage Waterways Council. 6PPD-quinone and its impact on coho salmon, 2021 [cited October 30, 2023]. Available from: https://www.anchoragecreeks.org/single-project.

(8) Klöckner, P.; Seiwert, B.; Wagner, S.; Reemtsma, T. Organic Markers of Tire and Road Wear Particles in Sediments and Soils: Transformation Products of Major Antiozonants as Promising Candidates. *Environ. Sci. Technol.* **2021**, *55* (17), 11723−11732.

(9) Ruggerone, G. T.; Peterman, R. M.; Dorner, B.; Myers, K. W. Magnitude and trends in abundance of hatchery and wild pink salmon, chum salmon, and sockeye salmon in the North Pacific Ocean. *Marine and Coastal Fisheries* **2010**, *2* (1), 306−328.

(10) Clay, S. A.; Koskinen, W. C.; Baker, J. M. Alachlor and metolachlor movement during winter and early spring at three Midwestern sites 1. *Journal of Environmental Science & Health Part B* **1995**, *30* (5), 637−650.

(11) Newton, M.; Cole, E. C.; Tinsley, I. J. Dissipation of four forest-use herbicides at high latitudes. *Environmental Science and Pollution Research* **2008**, *15* (7), 573−583.

(12) Ranft, R. D.; Seefeldt, S. S.; Zhang, M.; Barnes, D. L. Development of a soil bioassay for triclopyr residues and comparison with a laboratory extraction. *Weed technology* **2010**, *24* (4), 538−543.

(13) Tomco, P. L.; Duddleston, K. N.; Schultz, E. J.; Hagedorn, B.; Stevenson, T. J.; Seefeldt, S. S. Field degradation of aminopyralid and clopyralid and microbial community response to application in Alaskan soils. *Environmental toxicology and chemistry* **2016**, *35* (2), 485−493.

(14) Locatelli, M.; Carlucci, G.; Genovese, S.; Curini, M.; Epifano, F. Use of HPLC in the determination of the molar absorptivity of 4′-geranyloxyferulic acid and boropinic acid. *Chromatographia* **2011**, *73*, 889−896.

(15) Pelillo, M.; Cuvelier, M. E.; Biguzzi, B.; Toschi, T. G.; Berset, C.; Lercker, G. Calculation of the molar absorptivity of polyphenols by using liquid chromatography with diode array detection: the case of carnosic acid. *Journal of chromatography A* **2004**, *1023* (2), 225−229.

(16) Dissing, D.; Wendler, G. Solar radiation climatology of Alaska. *Theoretical and Applied Climatology* **1998**, *61* (3), 161−175.

(17) Whisenhant, E. A.; Zito, P.; Podgorski, D. C.; McKenna, A. M.; Redman, Z. C.; Tomco, P. L. Unique molecular features of water-soluble photo-oxidation products among refined fuels, crude oil, and herded burnt residue under high latitude conditions. *ACS ES&T Water* **2022**, *2* (6), 994−1002.

(18) Harsha, M. L.; Redman, Z. C.; Wesolowski, J.; Podgorski, D. C.; Tomco, P. L. Photochemical formation of water-soluble oxyPAHs, naphthenic acids, and other hydrocarbon oxidation products from Cook Inlet, Alaska crude oil and diesel in simulated seawater spills. *Environmental Science: Advances* **2023**, *2* (3), 447−461.

(19) Redman, Z. C.; Wesolowski, J.; Tomco, P. L. Photochemical Pathways of Rotenone and Deguelin Degradation: Implications for Rotenoid Attenuation and Persistence in High-Latitude Lakes. *Environ. Sci. Technol.* **2021**, *55* (8), 4974−4983.
(20) Boreen, A. L.; Edhlund, B. L.; Cotner, J. B.; McNeill, K. Indirect photodegradation of dissolved free amino acids: the contribution of singlet oxygen and the differential reactivity of DOM from various sources. *Environ. Sci. Technol.* **2008**, *42* (15), 5492−5498.
(21) Fellman, J. B.; D'Amore, D. V.; Hood, E. An evaluation of freezing as a preservation technique for analyzing dissolved organic C, N and P in surface water samples. *Science of the total environment* **2008**, *392* (2−3), 305−312.
(22) Di, S.; Liu, Z.; Zhao, H.; Li, Y.; Qi, P.; Wang, Z.; Xu, H.; Jin, Y.; Wang, X. Chiral perspective evaluations: Enantioselective hydrolysis of 6PPD and 6PPD-quinone in water and enantioselective toxicity to Gobiocypris rarus and Oncorhynchus mykiss. *Environ. Int.* **2022**, *166*, No. 107374.
(23) McKay, G.; Rosario-Ortiz, F. L. Temperature dependence of the photochemical formation of hydroxyl radical from dissolved organic matter. *Environ. Sci. Technol.* **2015**, *49* (7), 4147−4154.
(24) Hilpern, J. W.; Porter, G.; Stief, L. J. Decay of the triplet state I. First-order processes in solution. *Proc. R. Soc. London, Ser. A* **1964**, *277*, 437−447.
(25) Li, Z.; Bruce, A.; Galley, W. C. Temperature dependence of the disulfide perturbation to the triplet state of tryptophan. *Biophys. J.* **1992**, *61*, 1364−1371.
(26) McLean, A. J.; Rodgers, M. A. J. Variable-temperature study of aromatic hydrocarbon triplet-state quenching by molecular oxygen in solution. *J. Am. Chem. Soc.* **1993**, *115*, 4786−4792.
(27) Alegría, A. E.; Ferrer, A.; Santiago, G.; Sepúlveda, E.; Flores, W. Photochemistry of water-soluble quinones. Production of the hydroxyl radical, singlet oxygen and the superoxide ion. *J. Photochem. Photobiol., A* **1999**, *127* (1−3), 57−65.
(28) Rosario-Ortiz, F. L.; Canonica, S. Probe compounds to assess the photochemical activity of dissolved organic matter. *Environ. Sci. Technol.* **2016**, *50* (23), 12532−12547.
(29) Remke, S. C.; von Gunten, U.; Canonica, S. Enhanced transformation of aquatic organic compounds by long-lived photooxidants (LLPO) produced from dissolved organic matter. *Water Res.* **2021**, *190*, No. 116707.
(30) Weiner, S. A.; Mahoney, L. R. Mechanistic study of the termination reactions of 2, 4, 6-trialkylphenoxy radicals carboxylic acids. *J. Am. Chem. Soc.* **1972**, *94* (14), 5029−5033.
(31) Sanchez-Cruz, P.; Santos, A.; Diaz, S.; Alegría, A. E. Metal-independent reduction of hydrogen peroxide by semiquinones. *Chem. Res. Toxicol.* **2014**, *27* (8), 1380−1386.
(32) Zhu, B. Z.; Kalyanaraman, B.; Jiang, G. B. Molecular mechanism for metal-independent production of hydroxyl radicals by hydrogen peroxide and halogenated quinones. *Proc. Natl. Acad. Sci. U. S. A.* **2007**, *104* (45), 17575−17578.
(33) Gu, J.; Song, Y.; Yang, Y.; Guan, C.; Jiang, J. Mechanical insights into activation of peroxides by quinones: Formation of oxygen-centered radicals or singlet oxygen. *Environ. Sci. Technol.* **2022**, *56* (12), 8776−8783.
(34) Zhu, Y.; Powers, L. C.; Kieber, D. J.; Miller, W. L. Depth-resolved photochemical production of hydrogen peroxide in the global ocean using remotely sensed ocean color. *Frontiers in Remote Sensing* **2022**, *3*, No. 1009398.
(35) Mitroka, S.; Zimmeck, S.; Troya, D.; Tanko, J. M. How solvent modulates hydroxyl radical reactivity in hydrogen atom abstractions. *J. Am. Chem. Soc.* **2010**, *132* (9), 2907−2913.
(36) Hynes, A. J.; Wine, P. H. Kinetics and mechanism of the reaction of hydroxyl radicals with acetonitrile under atmospheric conditions. *J. Phys. Chem.* **1991**, *95* (3), 1232−1240.
(37) National Center for Atmospheric Research (NCAR). Atmospheric Chemistry Observations and Modeling Quick TUV Calculator, Boulder, CO, 2019 [cited July 3, 2023]. Available from: http://www.acom.ucar.edu/Models/TUV/Interactive_TUV/.
(38) Schymanski, E. L.; Jeon, J.; Gulde, R.; Fenner, K.; Ruff, M.; Singer, H. P.; Hollender, J. Identifying small molecules via high resolution mass spectrometry: communicating confidence. *Environ. Sci. Technol.* **2014**, *48*, 2097−2098.
(39) Seiwert, B.; Nihemaiti, M.; Troussier, M.; Weyrauch, S.; Reemtsma, T. Abiotic oxidative transformation of 6-PPD and 6-PPD quinone from tires and occurrence of their products in snow from urban roads and in municipal wastewater. *Water Res.* **2022**, *212*, No. 118122.
(40) Rossomme, E.; Hart-Cooper, W. M.; Orts, W. J.; McMahan, C. M.; Head-Gordon, M. Computational studies of rubber ozonation explain the effectiveness of 6PPD as an antidegradant and the mechanism of its quinone formation. *Environ. Sci. Technol.* **2023**, *57* (13), 5216−5230.
(41) Bhat, A. P.; Gogate, P. R. Degradation of nitrogen-containing hazardous compounds using advanced oxidation processes: a review on aliphatic and aromatic amines, dyes, and pesticides. *Journal of Hazardous Materials* **2021**, *403*, No. 123657.
(42) Lin, J.; Chen, J.; Wang, Y.; Cai, X.; Wei, X.; Qiao, X. More toxic and photoresistant products from photodegradation of fenoxaprop-p-ethyl. *Journal of agricultural and food chemistry* **2008**, *56* (17), 8226−8230.
(43) Yu, Y.; Zhou, D.; Wu, F. Mechanism and products of the photolysis of hexabromocyclododecane in acetonitrile−water solutions under a UV-C lamp. *Chemical Engineering Journal* **2015**, *281*, 892−899.
(44) Mushtaq, M.; Chukwudebe, A. C.; Wrzesinski, C.; Allen, L. R.; Luffer-Atlas, D.; Arison, B. H. Photodegradation of emamectin benzoate in aqueous solutions. *Journal of agricultural and food chemistry* **1998**, *46* (3), 1181−1191.

https://doi.org/10.1021/acs.est.3c05742
Environ. Sci. Technol. 2023, 57, 20813−20821